
The rms-flux relations in different branches in Cyg X-2

Z.B. Li¹ • L.M. Song² • J.L. Qu² • Y.J. Lei³ •
J.Y. Nie² • C.M. Zhang³

Abstract In this paper, the rms-flux (root mean square-flux) relation along the Z-track of the bright Z-Source Cyg X-2 is analyzed using the observational data of Rossi X-ray Timing Explorer (RXTE). Three types of rms-flux relations, i.e. positive, negative, and 'arch'-like correlations are found in different branches. The rms is positively correlated with flux in normal branch (NB), but anti-correlated in the vertical horizontal branch (VHB). The rms-flux relation shows an 'arch'-like shape in the horizontal branch (HB). We also try to explain this phenomenon using existing models.

Keywords stars: individual (Cyg X-2)–stars: neutron X-rays: stars

1 Introduction

Aperiodic X-ray variability is a common property in X-ray binaries (XRBs) and active galactic nuclei (AGN) (van der Klis 1994; Vaughan et al. 2003; McHardy et al. 2004). Many works have been done to investigate the aperiodic X-ray variability. For example, a linear correlation between rms (see Equation 1)

and flux of the X-ray in AGN and XRBs is reported by Uttley and McHardy (2001). This relation is found in both neutron star XRBs (NSXRBs) and black hole XRBs (BHXRBS) (Uttley and McHardy 2001; Li et al. 2010; Gleissner et al. 2004; Heil et al. 2011). Accordingly, the linear relation is supposed to be a fundamental property of accretion flows in compact objects. Recently, Heil and Vaughan (2010) report that this linear relation also exists in a Ultraluminous X-ray source, NGC 5408 X-1, which further strengthens the above supposition.

The rms-flux relation is very useful in evaluating X-ray variability models. Considering that the shot-noise model predicts a stationary power spectrum and can't produce a linear rms-flux relation, Uttley and McHardy (2001) pointed out that this model is not correct. Furthermore, Uttley (2004) showed that in the accreting millisecond pulsar SAX J1808.4-3658 is coupled with the 401-Hz pulsation. This indicates that the linear relation is not produced in the corona but in the accretion flow onto the magnetic caps of the neutron star (NS), which means that the linear relation does not favor the coronal flare model for the X-ray variability neither. Based on the investigation of the rms-flux linear relation on different time-scales, Uttley et al. (2005) ruled out several X-ray variability models except the perturbed accreting-flow model (e.g. density waves, Misra (2000)) of Lyubarskii (1997). On the other hand, Zhang (2007) found a similar rms-flux relation in the Sun and γ -ray bursts, suggesting that the accreting-flow model may be also wrong for the X-ray emission since the Sun does not have accretion flows. In conclusion, the rms-flux relation is very important in distinguishing X-ray variability models.

Gleissner et al. (2004) investigated the rms-flux relation in all known spectral states of a BHXRBS, Cyg X-1, and found that the linear relation exists in all spectral

Z.B. Li
lizhibing@xao.ac.cn

L.M. Song
J.L. Qu
Y.J. Lei
J.Y. Nie
C.M. Zhang

¹Xinjiang Astronomical Observatory, Chinese Academy of Sciences, 150, Science 1-Street, Urumqi, Xinjiang 830011, China

²Key Laboratory for Particle Astrophysics, Institute of High Energy Physics, Chinese Academy of Sciences, 19B YuQuan Road, Beijing, 100049, China

³National Astronomical Observatories, Chinese Academy of Sciences, Beijing, 100012, China

states although their power density spectra (PDS) show rather different shapes (Gleissner et al. 2004). This result implies that the rms-flux relation is a more universal characteristic than PDS shape.

Cyg X-2 is a bright, persistent low mass XRB (LMXB) (Bradt and McClintock 1983). It contains a NS (Kahn and Grindlay 1984), with an optically measured mass of $\sim 1.78 \pm 0.23 M_{\odot}$ and distance of 7.2 ± 1.1 kpc (Orosz and Kuulkers 1999). The orbital period is ~ 9.8 days (Cowley et al. 1979; Casares et al. 1998). For comparing the differences between a BHXR and a NSXR, we will investigate the rms-flux relations of different states in Cyg X-2 to check out whether the linear relation is valid or not throughout all the states of a NSXR.

Cyg X-2 is a Z source according to its track through different spectral states on the color-color diagram (CCD) (Hasinger and van der Klis 1989; Hasinger 1990; van der Klis 2000). In general, a Z source has three branches, i.e. the horizontal branch (HB), normal branch (NB) and flaring branch (FB). The HB usually locates at the top of the CCD, followed by the NB crossing the diagonal, and the so-called FB lies at the bottom of the CCD. Usually, a Z source can trace out a Z-track in few hours, but the Z-track will shift in weeks or months. Sometimes, the HB may have two portions: one is horizontal and the other is vertical. We call this vertical portion vertical horizontal branch (VHB) (Shirey 1998; Kuulkers et al. 1999; Shirey et al. 1999). During the evolution of a Z-source, it moves continuously on the Z-track, due to different mass accretion rate (van der Klis 2000). From simultaneous multi-band observations, it is thought that the mass accretion rate reaches a minimum at the left end of the HB, increases as the source travels from HB, throughout NB, to FB, and reaches its maximum at the right end of the FB (Hasinger and van der Klis 1989; Hasinger 1990). However, Church et al. (2006) has a different opinion about the mass accretion rate (see Church et al. (2006) and reference therein).

Cyg X-2 varies on time-scales from milliseconds to months (Kuulkers et al. 1996; Wijnands et al. 1996). Several kinds of quasi-periodic oscillations (QPOs) are detected in Cyg X-2 and its rapid variability is also found to be related with its position in the CCD. The QPOs that appear in the HB and the upper NB are called HB oscillations with the centroid frequency varying from ~ 10 Hz to ~ 70 Hz. The NB oscillations locate in the lower NB with the centroid frequency at ~ 5 -7 Hz (Hasinger and van der Klis 1989; van der Klis 2000; Piraino et al. 2002; van der Klis 2004). In addition, some kHz QPOs are observed in Cyg X-2 when the source moves from the left end of the HB to the upper NB (Wijnands et al. (1998) and references therein).

Section 2 is data reduction. The rms-flux relations are given in Section 3. Discussions are presented in Section 4.

2 Observations and data analysis

The observational data we used here are from RXTE archive, and are reduced by standard Heasoft package released by HEASARC.

2.1 Observations

In order to investigate the rms-flux relation in different branches, we require the exposure time as long as possible. Taking into account that the time interval Cyg X-2 stays in only one branch is $\sim 10\,000$ s, we use only those observations whose duration is longer than 10 000 s. Moreover, we discard those observations with different number of PCUs switched on during the observation (see *The RXTE Cook Book*) and also those observations locate at the FB or at the lower part of NB, since their PDS always have negative Power Density in the frequency range we are interested in. We list the observation IDs of the satisfactory observations in Table 1.

The first 7 observations belong to Epoch II and the other are during Epoch III. Their durations are longer than 10ks. In ObsIDs 10065-02-01-000 and 10065-02-01-001, the event mode data, E_125us_64M_0_1s, are used for investigation while the binned mode data, B_2ms_16A_0_35_Q, are used in the other 14 observations. We also list the location by their CCD position and PDS.

The CCDs of each observation are made by using the Standard 2 mode data with time resolution 16 s. We define the soft color as the count-rate ratio between 4.7-7.5 keV and 2.0-4.7 keV, and the hard color between 11.2-18.8 keV and 7.5-11.2 keV during Epoch II (see also Lei et al. (2008)). Because the PCU gains are different for different Epoches (see *The RXTE Cook Book*), the soft and hard colors of Epoch III are defined a little different from that of Epoch II, i.e., the count-rate ratio between 4.1-6.2 keV and 2.0-4.1 keV, and between 9.4-15.9 keV and 6.2-9.4 keV for soft and hard colors respectively. However, the difference is corrected using the Crab observations. All the above count rates are background-subtracted. The PDS of all the observations are extracted from the Binned Mode or Event Encoded mode (see Table 1) to locate their positions in CCD. The branches of those observations are listed in Table 1.

2.2 rms calculation

The Binned Mode or Event Encoded mode data are also used to obtain the rms-flux relations. For each observation, First, we extract the 4 ms time bin resolution light curve of Channel 0-35 (corresponding to 2-11.2 keV, 2-13 keV for Epoch II and Epoch III respectively). Second, we divide the light curve into 32s segments and sort them by their count rate. Third, we average these segments into several flux bins in order of the count rate with each flux bin contains ~ 20 segments (Actually the rms-flux relation does not vary with the time-scale of the flux bin, this is also consistent with the result in Cyg X-1 that the linear rms-flux relation is valid not only on short time-scales but also on longer time-scales, see Gleissner et al. (2004)). Fourth, we produce the PDSs of flux bins using the program 'POWSPEC 1.0' with the Poisson noise subtracted and the power normalized to squared mean intensity ((Miyamoto et al. 1991)). Finally, we integrate the power in a certain frequency range and multiply the square root of the integral value by the flux (count rate) of the flux bin, i.e.,

$$\sigma = \left\{ \int_{f_1}^{f_2} \langle P(f) \rangle df \right\}^{1/2} F, \quad (1)$$

where σ means the absolute rms, $\langle P(f) \rangle$ is the average power of a flux bin, which can read out from the PDS, and F is the count rate of the flux bin (normalized to one PCU), f_1 and f_2 are the lower and upper integral limits fixed at 0.125 Hz and 60 Hz respectively so as to include the contribution of QPOs. In this way, we can get the rms and flux of all the flux bins of an observation and thus derive the rms-flux relation.

The error of rms is given by the following equation:

$$(\Delta\sigma)^2 = \left(\frac{\partial\sigma}{\partial P(f)} \right)^2 (\Delta P(f))^2 + \left(\frac{\partial\sigma}{\partial F} \right)^2 (\Delta F)^2 \quad (2)$$

where $\Delta P(f)$ is error of $P(f)$, and ΔF is the error of the flux. As usual, we use the count rate of each flux bin as the flux ((Uttley and McHardy 2001; Gleissner et al. 2004; Li et al. 2010; Heil and Vaughan 2010)).

In this paper we have not corrected the effect of dead time of the instruments, because it accounts for only $\sim 1.2\%$ of the total rms and doesn't affect our results. (we use the dead time model of Zhang et al. (1995) to compute the instrumental dead time modification. See also equation (4) in Nowak et al. (1999).)

3 results

3.1 rms-flux relations in Proposal P10066

As an example, we will show the rms-flux relation of Proposal P10066 in this section, because it clearly shows three branches in the CCD. Proposal P10066 includes three observations, i.e. 10066-01-01-000, 10066-01-01-001 and 10066-01-01-00. We display its CCD and hard color-intensity diagram (HID) in Fig. 1. The CCD shows three branches clearly, i.e., the top, middle and bottom branch. Their PDS are shown in Fig. 2. Because both the top and middle branches exhibit QPOs between ~ 15 to ~ 60 Hz, they locate in the HB. Given the shape of the top branch, we name it VHB, and call the middle branch HB. The bottom branch is NB because of a power law PDS and its ~ 7 Hz QPO (see Hasinger and van der Klis (1989)). Using the method in Section 2.2, we obtain the rms-flux relations of the three branches, and the results are shown in Fig. 3.

Our analysis shows that the rms is negatively correlated with flux in the VHB, but positively correlated in the NB of P10066 (Fig. 3). In the HB of P10066, the rms-flux relation is not a linear correlation anymore. In fact, the rms positively correlated with flux in the left part of HB and negatively correlated in the right. In this manner the rms has a maximum value at the flux of ~ 1400 cts/s, approximately corresponding to the middle part of HB. For comparison we show the whole rms-flux relation of Proposal P10066 in Fig. 4. By using a linear model to fit the relation of each branch in Fig. 4, we derive the turn-over points between different branches. In the VHB of P10066, the flux is less than ~ 950 cts/s/pcu and the QPO frequency of each flux bin is less than ~ 30 Hz. In the left HB of P10066, the flux is more than ~ 950 cts/pcu and less than ~ 1430 cts/s/pcu, and its QPO frequency is between ~ 30 Hz and ~ 50 Hz. The flux of the right HB of P10066 is more than ~ 1430 cts/s/pcu and its QPO frequencies range from ~ 50 Hz to ~ 55 Hz. Those turn-over points are listed in Table 2.

3.2 rms-flux relations in the other observations

We derive the rms-flux relations of all the other observations listed in Table 1. The results are shown in Fig. 5-10. Fig. 5 show the results of ObsID 30046-01-12-00, who locates in the VHB of the CCD. Its flux bin frequencies and flux are respectively less than ~ 30 Hz and ~ 950 cts/s/pcu, and the rms-flux relation is negative. These results are similar to those of the VHB P10066. Fig. 6 shows the results of these observations locating in HB. Their rms-flux relations are the same as

in the HB of P10066. By fitting their rms-flux relations, we derive the turn-over points are ~ 1460 cts/s/pcu, ~ 1480 cts/s/pcu, ~ 1430 cts/s/pcu and ~ 1400 cts/s/pcu for 10065-02-01-000, 10065-02-01-001, 10065-02-01-002, and 10065-02-01-003, respectively. Moreover, their QPO frequencies are between ~ 38 Hz and ~ 50 Hz for the left HB, and between ~ 50 Hz and ~ 55 Hz for the right HB (Table 2). The ObsIDs 20053-04-01-010 and 20053-04-01-020 locate in the NB and their results are shown in Fig 7. There two observations do not have obvious QPOs but a bump at ~ 5 -7 Hz, and their hard colors are less than ~ 0.45 . Although their flux, between ~ 950 cts/s/pcu and ~ 1100 cts/s/pcu, are less than in the NB of P10066, their rms-flux relations are positive.

Fig. 8 shows the results of these observations locate only in the left part of HB. For the ObsID 30046-01-03-00, its flux is less than ~ 1300 cts/s/pcu and its frequency is between ~ 45 Hz and ~ 53 Hz. However, the situation is a little different for ObsID 300418-01-01-00. Its flux is less than ~ 1500 cts/s/pcu and the QPO frequencies range from ~ 30 Hz to ~ 48 Hz. As a result, their rms-flux relations are positive. There are three observations locate in the right part of HB (see Table 1) and their results are shown in Fig. 9. Their hard colors are more than ~ 0.45 while their flux are between ~ 800 cts/s/pcu and ~ 1100 cts/s/pcu. For ObsIDs 20053-04-01-03 and 20053-04-01-04, the QPO frequencies are around ~ 53 -55 Hz, but it locates around ~ 45 Hz in the ObsID 20053-04-01-030. The same as in the right HB of P10066, their rms are negatively correlated with flux. Because these observations shown in Fig. 8-9 occupy only a portion of HB, their rms-flux relations show only a portion of the arch-like relation of the HB of P10066 either.

In addition, there is one observation, 30046-01-08-00, locating at the vertex of the VHB and HB (see Fig. 10). This observation has two branches. The flux of the VHB part is less than ~ 960 cts/s/pcu, and its QPO frequencies range from ~ 26 Hz to ~ 35 Hz, while the flux of the left HB part is more than ~ 960 cts/s/pcu and its QPO frequencies are between ~ 37 Hz and ~ 50 Hz (see Table 2). As shown in the right panel of Fig. 10, the VHB part shows a negative correlation in the rms-flux plot, and the left HB part shows a positive one, which are consistent with those results above.

3.3 the correlations between rms and spectral parameters in P10066

Because the other observations have the same results of rms-flux relations as in Proposal P10066, our spectral fitting concentrate only on Proposal P10066. First, we split the data into 25 intervals according to its position on the CCD. The average hard color (HC) and

soft color (SC) of the 25 intervals are listed in Table 3. (Because there is no need to correct the gain difference between Epoches II and III, we haven't corrected the colors in this subsection and they are different from above.) Second, we compute their rms using the method described above (see Table 3). Finally, we extract their spectra with the Standard 2 mode data and use the X-ray spectral-fitting program, XSPEC, to analyze their spectra.

Considering the controversy over the location and nature of the X-ray emission regions, we fit their spectra with the Eastern and Western model, respectively. We use the absorbed disk blackbody, Comptonization plus an extra Gaussian line (wabs(diskbb+compTT+gauss)) as the Eastern model, and the absorbed blackbody, Comptonization plus an extra Gaussian line (wabs(bb+compTT+gauss)) as the Western model, i.e. the Birmingham model Church and Balucinska-Church (1995). The fitting energy band is 3-30keV and the absorption column density N_h is fixed at 0.2×10^{22} . According to their reduced χ^2 values shown in Table 3, we can find that the Western model gives a better fitting results for those intervals whose ID > 17 . We also give the inner radius of the accretion disk of the Eastern Model in Table 3 by assuming an inclination angle of the system of 60° (see (Di Salvo et al. 2002)). Because the inner disk radius is less than the typical radius of a NS, i.e., ~ 10 km, the Eastern Model isn't reasonable for Cyg X-2 in this situation. The spectral parameters of the Birmingham model are listed in Table 4. The relations between the rms and flux of these two components of Birmingham model is shown in Fig. 11. We also present the relation between the rms and flux ratio of blackbody and Comptonization components in Fig. 12.

4 Discussion

Li et al. (2010) firstly reported a negative rms-flux relation in Cyg X-2, and then it is also found in the black hole XRB XTE J1550-564 (see also Heil et al. (2011)). The positive relation can, in principle, be readily understood: the larger the flux, the higher the accretion rate which leads to a higher level of instability. Nevertheless, the negative correlation between rms and flux in Cyg X-2 and XTE J1550-564 is hard to fit into this scenario (see Li et al. (2010); Heil et al. (2011)). As shown in Fig. 10, the complicated rms-flux relation of Cyg X-2 leads to a maximal rms in the middle of HB, which means that Cyg X-2 has a maximum level of instability no matter how luminous it is. Moreover, the negative relation dose not change with the integral frequency range. In other words, if we do not include the

QPO and only integral from 0.125 Hz to 10 Hz when we compute the rms, the rms-flux relation is also negative in the VHB. This means that the negative relation is not caused by the QPO. We also normalize the rms by dividing the flux of each flux bin, and the normalized rms shows a positive correlation with flux in the NB, but negative in the VHB, which is totally the same as not normalized. The same results mean that the rms-flux relation isn't due to the flux change of different flux bins.

To compare NSXRB Cyg X-2 with BHXR B Cyg X-1, we investigate the rms-flux relations in different branches in Cyg X-2. As shown above, the rms is positively correlated with flux when Cyg X-2 locates in the NB or at the left part of HB. However, it is negatively correlated with flux in the VHB or at the right part of HB. This is different from those reported in Uttley and McHardy (2001); Uttley (2004); Heil and Vaughan (2010). Especially, Gleissner et al. (2004) found that the positive rms-flux relation is valid throughout all states of the BHXR B Cyg X-1. Moreover, the slope of the rms-flux relation of the hard state is steeper than in the soft and intermediate states of Cyg X-1. However, the slopes of the hard state (VHB state and its slope is negative) is flatter than in the soft state (NB state, its slope is positive) in Cyg X-2. We guess that this difference may come from the compact star.

However, although Cyg X-1 and Cyg X-2 have different results in the hard and soft states, the rms-flux relation shows some similarities if we assume HB is the intermediate state of Cyg X-2. Gleissner et al. (2004) reported an 'arch'-like rms-flux relation in the intermediate state of Cyg X-1, but they claimed that the 'arch' relation is due to the buffer overflow.

The so-called buffer overflow occurs when a program or process tries to store more data in a buffer (temporary data storage area) than it could hold. Due to the softness of the X-ray spectrum, the likelihood for such overflows is the highest in the lowest energy band. Still, for the different configuration, the possibility of overflow is lower when the configuration threshold is higher. In this work, we also find some 'arch' relations in the intermediate state of Cyg X-2 and try to determine whether the arch shape in Cyg X-2 is due to the buffer overflow or not. We've tried the Event Encoded mode data (see Table 1 and Fig. 6), the higher threshold mode data, and higher energy band data, which are less likely suffered from buffer overflows (also see http://heasarc.gsfc.nasa.gov/docs/xte/RXTE_tech_append.pdf), and found that these data also show similar arch relations. On the other hand, we've done some simulations and the simulation results don't support

the argue that the arch relation is due to the buffer overflow. As a result, we conclude that the 'arch' rms-flux relation may be the characteristic of the state transition, which always take place at the QPO frequency ~ 50 Hz (see Table 2).

In the 1980s, two models were proposed to explain the X-ray emission of the NSXRB: the Western model and the Eastern model. The Eastern model contains a multi-temperature blackbody from the inner disc, plus a Comptonized emission of the seed photons from the blackbody of the NS (Mitsuda et al. 1989), while the Western model contains a Comptonization component and sometimes a second one (i.e., blackbody emission) for some luminous sources (White et al. 1988). In the 1990s, a new model - the Birmingham model, closely related to the Western model - is proposed. This model assumes that all LMXBs have two continuum components: blackbody emission from the NS surface and Comptonized emission from an extended accretion disc corona above the accretion disc (Church and Balucinska-Church 1995). Our spectral results show that the Birmingham model is more reasonable than the Eastern model (see Table 3), and this suggests that the two components in Cyg X-2 are most likely the blackbody coming from the surface of the NS and the Comptonization generated from the corona.

From Table 4 we know that the temperatures of the seed photons, the blackbody and the corona, the optical depth, and the flux of the Comptonization component change little, while the blackbody flux increases apparently in the VHB. A scenario hinted from these results may be that the corona is not efficiently cooled by the soft disk emission, and the latter is also likely stable because of the little change in T_0 . As a result most material move onto the surface of NS, and the rms changes obviously. In other words, the negative rms-flux relation of the VHB is supposed to contribute from the blackbody component (Fig. 11). Similarly, the rms is dominated by the Comptonization component in the NB (Fig. 11). To sum up, the blackbody component dominates the rms variability in VHB and its contribution to rms decreases as Cyg X-2 evolving through the HB to NB, whereas the rms contributed by the Comptonization component increases and dominates the rms variability in NB at last. This inference is also supported by the results that the rms negatively correlated with flux in energy bands 2-6keV and 6-10keV, and positively correlated in 10-21keV (see Li et al. (2010)). Because of these totally different manners of these two components, Cyg X-2 has a complex rms-flux relation along with the CCD track.

Fig. 12 shows that the instability of Cyg X-2 is related to the flux ratio between the blackbody and

Comptonization components. Only when those two components reach a certain ratio, Cyg X-2 reaches its maximum instability. This can be explained in the Birmingham model. In this model, the radiation of the blackbody shines on the accretion disc and forms a corona. On the one hand, the rms produced by the blackbody decreases when the flux of the blackbody increases. On the other hand, the radiation of the increasing blackbody will expand the corona region and increase the flux of the Comptonization component, which will finally increase its rms. As a result, the rms has a maximum only when their flux reaches a certain ratio.

Acknowledgements This work is subsidized by the Program of the Light in Chinese Western Region (LCWR) (Grant No. XBBS201121) provided by Chinese Academy of Sciences (CAS), the Natural Science Foundation of China for support via NSFC 11173034, 10903005, 11173024, 10473010 and 19673010, CAS key project via KJCX2-YWT03 and National Basic Research Program of China (2009CB824800). We thank S. N. Zhang, H. Tong, F. J. Lu, Y. P. Chen, S. J. Zheng, and M. Y. Ge for useful discussions.

References

- Bradt, H.V.D., McClintock, J.E.: *Annu. Rev. Astron. Astrophys.* **21**, 13 (1983). doi:10.1146/annurev.aa.21.090183.000305
- Casares, J., Charles, P.A., Kuulkers, E.: *Astrophys. J. Lett.* **493**, 39 (1998). arXiv:astro-ph/9711236. doi:10.1086/311124
- Church, M.J., Balucinska-Church, M.: *Astron. Astrophys.* **300**, 441 (1995)
- Church, M.J., Halai, G.S., Bałucińska-Church, M.: *Astron. Astrophys.* **460**, 233 (2006). arXiv:astro-ph/0609821. doi:10.1051/0004-6361/20065035
- Cowley, A.P., Crampton, D., Hutchings, J.B.: *Astrophys. J.* **231**, 539 (1979). doi:10.1086/157216
- Di Salvo, T., Farinelli, R., Burderi, L., Frontera, F., Kuulkers, E., Masetti, N., Robba, N.R., Stella, L., van der Klis, M.: *Astron. Astrophys.* **386**, 535 (2002). arXiv:astro-ph/0202295. doi:10.1051/0004-6361:20020238
- Geissner, T., Wilms, J., Pottschmidt, K., Uttley, P., Nowak, M.A., Staubert, R.: *Astron. Astrophys.* **414**, 1091 (2004). arXiv:astro-ph/0311039. doi:10.1051/0004-6361:20031684
- Hasinger, G.: In: G. Klare (ed.) *Reviews in Modern Astronomy. Reviews in Modern Astronomy*, vol. 3, p. 60 (1990)
- Hasinger, G., van der Klis, M.: *Astron. Astrophys.* **225**, 79 (1989)
- Heil, L.M., Vaughan, S.: *Mon. Not. R. Astron. Soc.* **405**, 86 (2010). 1003.5825. doi:10.1111/j.1745-3933.2010.00864.x
- Heil, L.M., Vaughan, S., Uttley, P.: *Mon. Not. R. Astron. Soc.* **411**, 66 (2011). 1011.6321. doi:10.1111/j.1745-3933.2010.00997.x
- Kahn, S.M., Grindlay, J.E.: *Astrophys. J.* **281**, 826 (1984). doi:10.1086/162161
- Kuulkers, E., van der Klis, M., Vaughan, B.A.: *Astron. Astrophys.* **311**, 197 (1996)
- Kuulkers, E., Wijnands, R., van der Klis, M.: *Mon. Not. R. Astron. Soc.* **308**, 485 (1999). arXiv:astro-ph/9904352. doi:10.1046/j.1365-8711.1999.02751.x
- Lei, Y.J., Qu, J.L., Song, L.M., Zhang, C.M., Zhang, S., Zhang, F., Wang, J.M., Li, Z.B., Zhang, G.B.: *Astrophys. J.* **677**, 461 (2008). 0801.3329. doi:10.1086/533423
- Li, Z., Lei, Y., Qu, J., Zhang, S., Song, L.: *Science in China G: Physics and Astronomy* **53**, 86 (2010). doi:10.1007/s11433-010-0007-3
- Lyubarskii, Y.E.: *Mon. Not. R. Astron. Soc.* **292**, 679 (1997)
- McHardy, I.M., Papadakis, I.E., Uttley, P., Page, M.J., Mason, K.O.: *Mon. Not. R. Astron. Soc.* **348**, 783 (2004). arXiv:astro-ph/0311220. doi:10.1111/j.1365-2966.2004.07376.x
- Misra, R.: *Astrophys. J. Lett.* **529**, 95 (2000). arXiv:astro-ph/9912177. doi:10.1086/312470
- Mitsuda, K., Inoue, H., Nakamura, N., Tanaka, Y.: *Publ. Astron. Soc. Jpn.* **41**, 97 (1989)
- Miyamoto, S., Kimura, K., Kitamoto, S., Dotani, T., Ebisawa, K.: *Astrophys. J.* **383**, 784 (1991). doi:10.1086/170837
- Orosz, J.A., Kuulkers, E.: *Mon. Not. R. Astron. Soc.* **305**, 132 (1999). arXiv:astro-ph/9901177. doi:10.1046/j.1365-8711.1999.t011-1-02420.x
- Palumbo, S., Santangelo, A., Kaaret, P.: *Astrophys. J.* **567**, 1091 (2002). doi:10.1086/338037
- Shirey, R.E.: *Mass Transfer and Accretion in the Eccentric Neutron-Star Binary Circinus X-1*. PhD thesis, Massachusetts Institute of Technology, (1998) (June 1998)
- Shirey, R.E., Bradt, H.V., Levine, A.M.: *Astrophys. J.* **517**, 472 (1999). arXiv:astro-ph/9901003. doi:10.1086/307188
- Uttley, P.: *Mon. Not. R. Astron. Soc.* **347**, 61 (2004). arXiv:astro-ph/0311453. doi:10.1111/j.1365-2966.2004.07434.x
- Uttley, P., McHardy, I.M.: *Mon. Not. R. Astron. Soc.* **323**, 26 (2001). arXiv:astro-ph/0103367. doi:10.1046/j.1365-8711.2001.04496.x
- Uttley, P., McHardy, I.M., Vaughan, S.: *Mon. Not. R. Astron. Soc.* **359**, 345 (2005). arXiv:astro-ph/0502112. doi:10.1111/j.1365-2966.2005.08886.x
- van der Klis, M.: *Astrophys. J. Suppl. Ser.* **92**, 511 (1994). doi:10.1086/192006
- van der Klis, M.: *Annu. Rev. Astron. Astrophys.* **38**, 717 (2000). arXiv:astro-ph/0001167. doi:10.1146/annurev.astro.38.1.717
- van der Klis, M.: *ArXiv Astrophysics e-prints* (2004). arXiv:astro-ph/0410551
- Vaughan, S., Fabian, A.C., Nandra, K.: *Mon. Not. R. Astron. Soc.* **339**, 1237 (2003). arXiv:astro-ph/0211421. doi:10.1046/j.1365-8711.2003.06285.x
- White, N.E., Stella, L., Parmar, A.N.: *Astrophys. J.* **324**, 363 (1988). doi:10.1086/165901
- Wijnands, R.A.D., Kuulkers, E., Smale, A.P.: *Astrophys. J. Lett.* **473**, 45 (1996). doi:10.1086/310390
- Wijnands, R., Homan, J., van der Klis, M., Kuulkers, E., van Paradijs, J., Lewin, W.H.G., Lamb, F.K., Psaltis, D., Vaughan, B.: *Astrophys. J. Lett.* **493**, 87 (1998). arXiv:astro-ph/9711219. doi:10.1086/311138
- Zhang, S.N.: *Highlights of Astronomy* **14**, 41 (2007). arXiv:astro-ph/0702246. doi:10.1017/S1743921307009842
- Zhang, W., Jahoda, K., Swank, J.H., Morgan, E.H., Giles, A.B.: *Astrophys. J.* **449**, 930 (1995). doi:10.1086/176111

This manuscript was prepared with the AAS L^AT_EX macros v5.2.

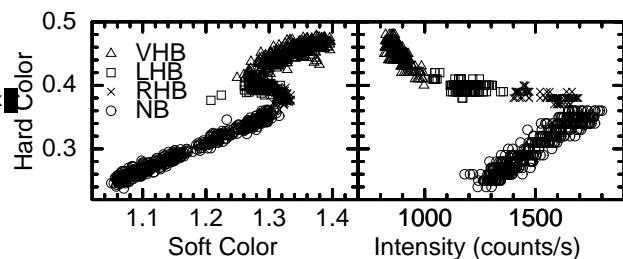


Fig. 1 The CCD (left panel) and HID (right panel) of Proposal P10066. The hard and soft color is defined as the flux ratio between 11.2-18.8keV and 7.5-11.2keV, and between 4.7-7.5keV and 2-4.7keV, respectively. The Intensity is defined as the count rate of 2-18.8keV.

Table 1 The information of those observations used in this work.

ObsID	date	epoch	duration	data mode	Branch
10065-02-01-000	23/3/96	II	14ks	E_125us_64M_0_1s	HB
10065-02-01-001	23/3/96	II	25ks	E_125us_64M_0_1s	HB
10065-02-01-002	23/3/96	II	19ks	B_2ms_16A_0_35_Q	HB
10065-02-01-003	23/3/96	II	15ks	B_2ms_16A_0_35_Q	HB
10066-01-01-00	27/3/96	II	16ks	B_2ms_16A_0_35_Q	VHB
10066-01-01-000	26/3/96	II	16ks	B_2ms_16A_0_35_Q	NB
10066-01-01-001	27/3/96	II	18ks	B_2ms_16A_0_35_Q	HB
20053-04-01-010	1/7/97	III	25ks	B_2ms_16A_0_35_Q	NB
20053-04-01-020	1/7/97	III	15ks	B_2ms_16A_0_35_Q	NB
20053-04-01-03	2/7/97	III	12ks	B_2ms_16A_0_35_Q	right HB
20053-04-01-030	2/7/97	III	13ks	B_2ms_16A_0_35_Q	right HB
20053-04-01-04	2/7/97	III	15ks	B_2ms_16A_0_35_Q	right HB
30046-01-03-00	28/7/98	III	15ks	B_2ms_16A_0_35_Q	left HB
30046-01-08-00	30/8/98	III	12ks	B_2ms_16A_0_35_Q	VHB-HB vertex
30046-01-12-00	25/9/98	III	20ks	B_2ms_16A_0_35_Q	VHB
30418-01-01-00	2/7/98	III	12ks	B_2ms_16A_0_35_Q	left HB

Table 2 The turn-over points between different branches. R and f stand for the flux in the unit of cts/s/pcu and the frequency of the QPO or the bump in the unit of Hz, respectively.

ObsID	VHB	left HB	right HB	NB
10065-02-01-000	—	$R < 1460, 38 < f < 50$	$1460 < R, 50 < f < 55$	—
10065-02-01-001	—	$R < 1480, 38 < f < 50$	$1480 < R, 50 < f < 55$	—
10065-02-01-002	—	$R < 1430, 38 < f < 50$	$1430 < R, 50 < f < 55$	—
10065-02-01-003	—	$R < 1400, 38 < f < 50$	$1400 < R, 50 < f < 55$	—
VHB of P10066	$R < 950, f < 30$	—	—	—
left HB of P10066	—	$950 < R < 1430, 30 < f < 50$	—	—
right HB of P10066	—	—	$1430 < R, 50 < f < 55$	—
NB of P10066	—	—	—	$5 < f < 7$
20053-04-01-010	—	—	—	$5 < f < 7$
20053-04-01-020	—	—	—	$5 < f < 7$
20053-04-01-03	—	—	$800 < R < 1100, f \sim 53-55$	—
20053-04-01-030	—	—	$800 < R < 1100, f \sim 53-55$	—
20053-04-01-04	—	—	$800 < R < 1100, f \sim 45$	—
30046-01-03-00	—	$R < 1300, 45 < f < 53$	—	—
30046-01-08-00	$R < 960, 26 < f < 35$	$960 < R, 37 < f < 50$	—	—
30046-01-12-00	$R < 950, f < 30$	—	—	—
30418-01-01-00	—	$R < 1500, 30 < f < 48$	—	—

Table 4 The fitting parameters of the Birmingham model. The fitting energy band is 3-30keV and the absorption column density N_h is fixed at 0.2×10^{22} .

ID	T_0^1	T_{bb}^1	kT^1	τ^2	Fe^3	$flux_{bb}^4$	$flux_{compTT}^4$	$flux_{total}^4$
1	0.183±0.005	1.39±0.07	3.11±0.05	5.67±0.16	6.44±0.09	1.06	6.65	7.84±0.01
2	0.194±0.004	1.27±0.05	3.02±0.04	5.94±0.12	6.46±0.09	0.99	6.81	7.96±0.01
3	0.202±0.004	1.26±0.05	3.03±0.04	5.91±0.12	6.49±0.08	1.07	6.77	8.00±0.01
4	0.186±0.004	1.26±0.05	3.02±0.04	5.89±0.13	6.58±0.08	1.13	6.76	8.02±0.01
5	0.254±0.003	1.26±0.04	3.01±0.04	5.90±0.12	6.50±0.08	1.13	6.80	8.07±0.01
6	0.202±0.004	1.29±0.05	3.02±0.05	5.80±0.14	6.48±0.08	1.17	6.84	8.13±0.01
7	0.253±0.003	1.21±0.03	2.96±0.03	5.91±0.11	6.56±0.09	1.32	6.78	8.23±0.01
8	0.215±0.003	1.19±0.03	2.94±0.03	5.89±0.10	6.49±0.09	1.33	6.82	8.28±0.01
9	0.178±0.002	1.17±0.03	2.93±0.02	5.95±0.10	6.59±0.08	1.43	6.80	8.35±0.01
10	0.214±0.003	1.21±0.03	2.95±0.03	5.77±0.11	6.50±0.10	1.60	6.86	8.57±0.01
11	0.192±0.004	1.18±0.02	2.85±0.04	6.02±0.14	6.56±0.11	2.58	7.25	9.90±0.01
12	0.177±0.004	1.17±0.02	2.85±0.04	6.04±0.13	6.59±0.14	2.75	7.42	10.27±0.01
13	0.184±0.003	1.11±0.02	2.73±0.03	6.47±0.12	6.53±0.16	2.71	7.53	10.37±0.02
14	0.219±0.003	1.14±0.02	2.78±0.03	6.31±0.12	6.62±0.12	2.85	7.57	10.53±0.02
15	0.228±0.003	1.14±0.02	2.76±0.03	6.37±0.12	6.57±0.14	2.88	7.77	10.77±0.01
16	0.185±0.003	1.12±0.01	2.73±0.03	6.60±0.12	6.60±0.14	3.06	7.81	11.01±0.01
17	0.204±0.004	1.13±0.02	2.70±0.03	6.72±0.13	6.33±0.18	3.40	8.41	11.98±0.02
18	0.207±0.005	1.17±0.02	2.70±0.03	6.76±0.15	6.58±0.15	4.23	8.91	13.22±0.02
19	0.182±0.005	1.21±0.02	2.75±0.04	6.44±0.16	6.64±0.16	4.80	9.28	14.16±0.02
20	0.184±0.005	1.18±0.01	2.68±0.03	6.86±0.15	6.59±0.17	5.03	9.59	14.70±0.02
21	0.181±0.004	1.19±0.01	2.69±0.03	6.33±0.11	6.64±0.18	5.76	8.97	14.80±0.02
22	0.190±0.004	1.16±0.01	2.63±0.03	6.24±0.11	6.62±0.11	5.42	8.23	13.74±0.02
23	0.184±0.003	1.12±0.01	2.56±0.03	6.02±0.11	6.62±0.13	5.28	7.07	12.46±0.02
24	0.196±0.003	1.07±0.01	2.41±0.02	6.03±0.10	6.57±0.09	5.07	6.12	11.32±0.01
25	0.214±0.004	1.00±0.01	2.26±0.02	6.49±0.10	6.30±0.07	4.69	5.59	10.55±0.02

¹ Their units are keV and represent the temperature of seed photons, blackbody and the corona respectively.

² τ stands for the optical depth.

³ Fe denotes the energy of the iron line.

⁴ Their units are $10^{-9} \text{ ergs s}^{-1} \text{ cm}^{-2}$ and represent the 3-30keV flux of blackbody, Comptonization component and total flux respectively.

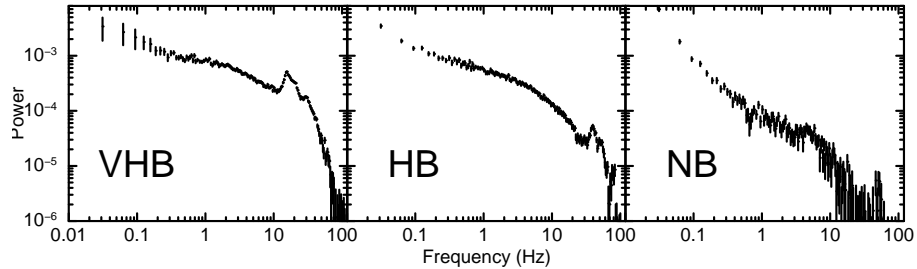


Fig. 2 The PDSs of VHB(left), HB(middle) and NB(right) for Proposal P10066.

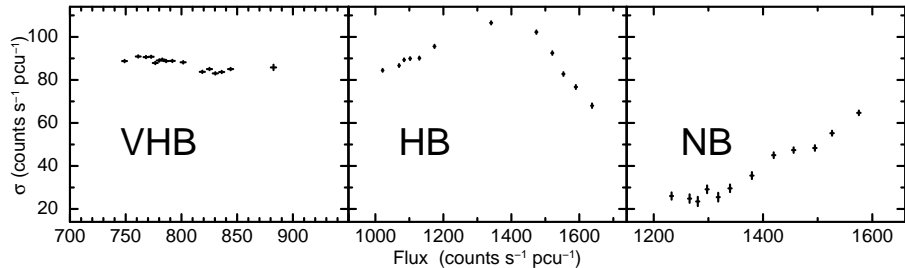


Fig. 3 The rms-flux relations of VHB(left), HB(middle) and NB(right) for Proposal P10066

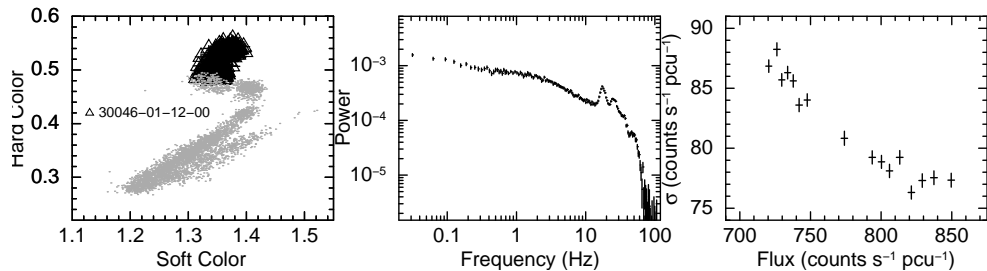


Fig. 5 This figure shows the CCD(left), PDS(middle) and rms-flux relation(right) of ObsID 30046-01-12-00, which locates at the VHB and displays a negative correlation.

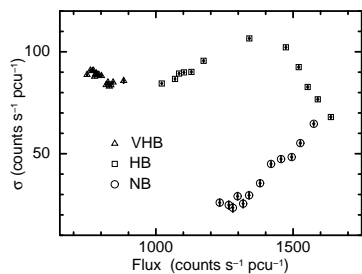


Fig. 4 The complete rms-flux relation of Proposal P10066.

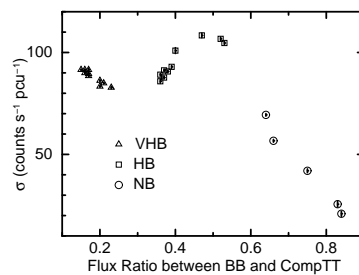


Fig. 12 The rms-ratio plot of Proposal P10066. The X-axis stands for its flux ratio between blackbody and Comptonization components.

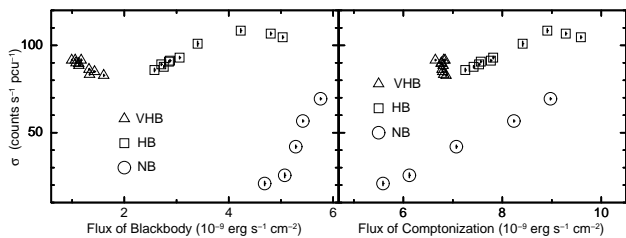


Fig. 11 The rms-flux plot. The X-axis of the left panel is the flux of blackbody, and the right is the flux of Comptonization component.

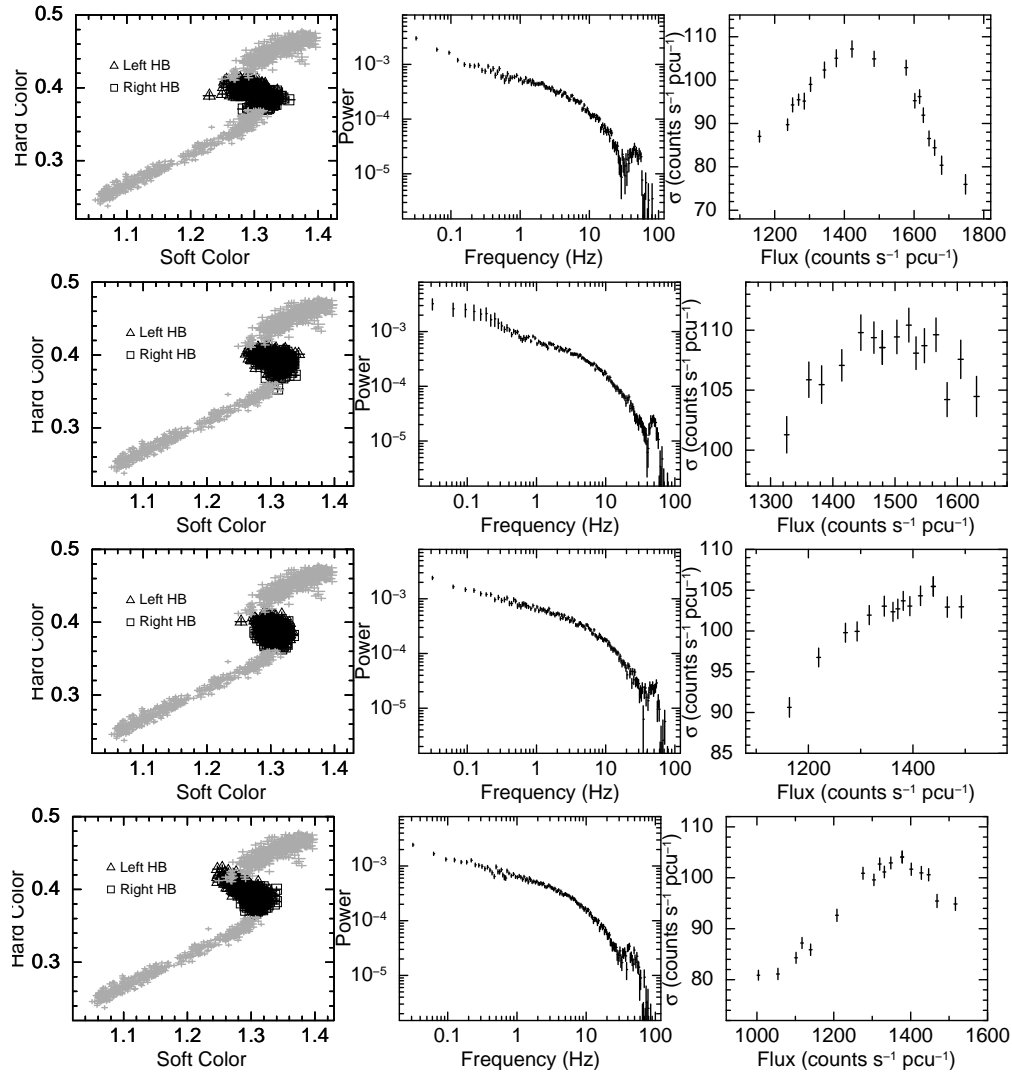


Fig. 6 The CCDs (left column), PDSs (middle column) and rms-flux relations (right column) of those observations locating at the HB. Row 1, 2, 3 and 4, show the results of ObsIDs 10065-02-01-000, 10065-02-01-001, 10065-02-01-002 and 10065-02-01-003, respectively. The left HB is marked with triangles and the right HB with squares in each CCD.

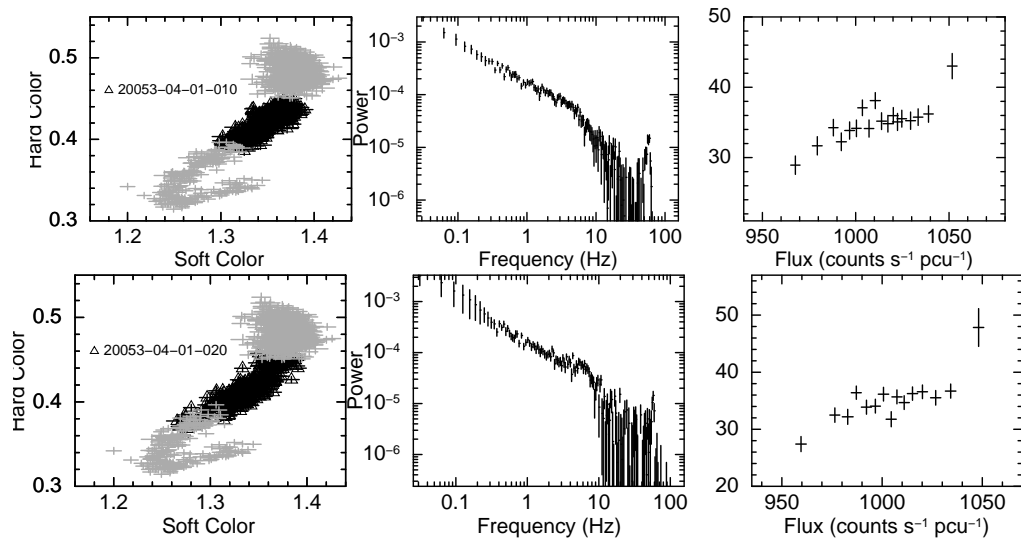


Fig. 7 The CCDs (left column), PDSs (middle column) and rms-flux relations (right column) of observations locate in the NB. The top and bottom panels show the results of ObsIDs 20053-04-01-010 and 20053-04-01-010 respectively.

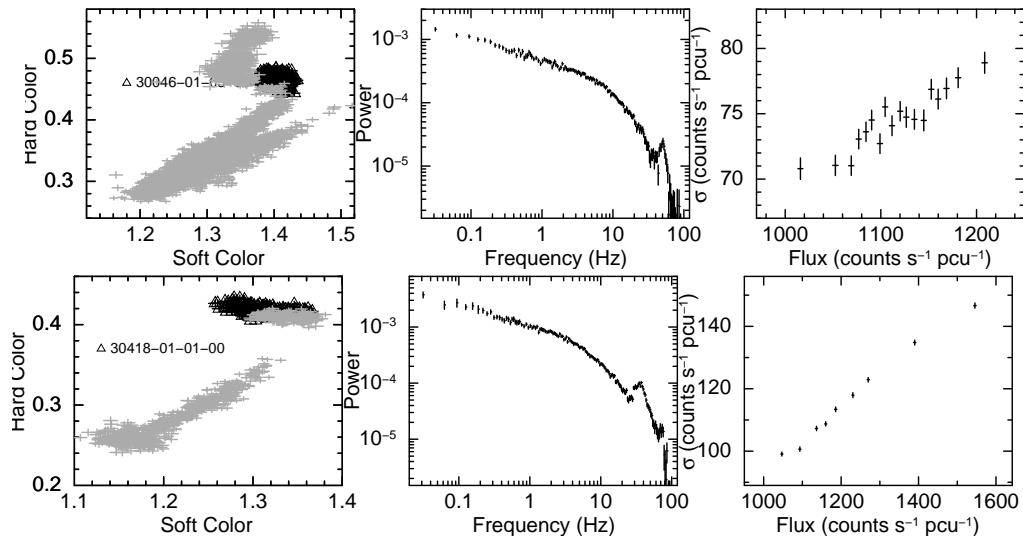


Fig. 8 The CCDs (left column), PDSs (middle column) and rms-flux relations (right column) of observations locate in the left part of HB. The top and bottom panels show the results of ObsIDs 30046-01-03-00 and 30418-01-01-00 respectively.

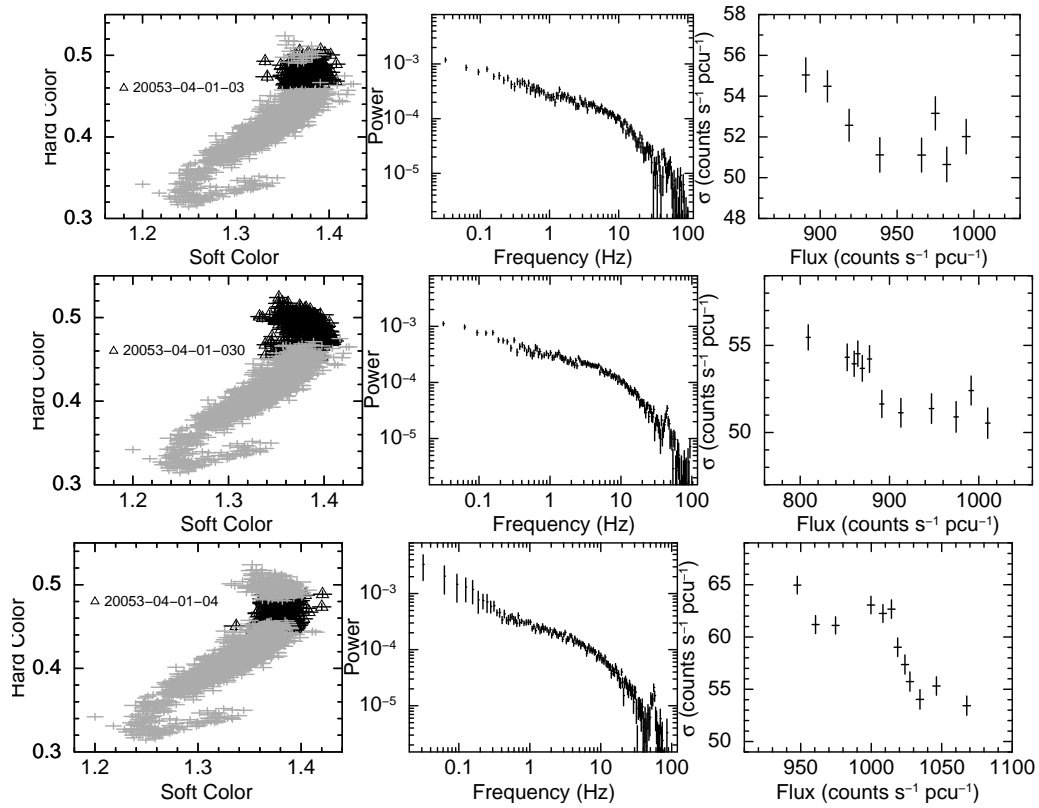


Fig. 9 The CCDs (left column), PDSs (middle column) and rms-flux relations (right column) of observations locate in the right part of HB. The top, middle and bottom panels show the results of ObsIDs 20053-04-01-03, 20053-04-01-030 and 20053-04-01-04, respectively.

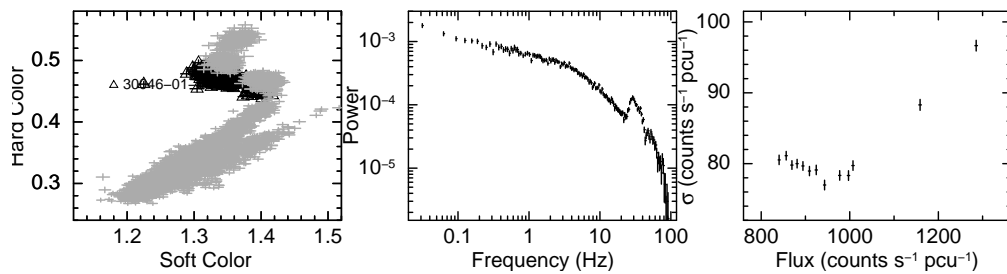


Fig. 10 The CCD (left), PDS (middle) and rms-flux relation (right) of ObsID 30046-01-08-00, which locates in the vertex of VHB and HB.

Table 3 The χ^2 of the Western and Eastern models. R_{in} is the inner disk radius derived from the Eastern Model by assuming an inclination angle of the system of 60° .

ID	HC	SC	Western ¹	Eastern ²	rms	R_{in} ³
1	0.395	0.885	0.92(56)	0.91(56)	91.5±0.4	3.3
2	0.394	0.885	0.83(56)	0.89(56)	91.5±0.4	4.2
3	0.391	0.883	0.89(56)	0.91(56)	90.0±0.4	4.6
4	0.389	0.875	1.18(56)	1.24(56)	89.6±0.4	4.3
5	0.389	0.876	1.06(56)	1.07(56)	88.5±0.4	4.7
6	0.386	0.872	0.80(56)	0.82(56)	91.5±0.7	4.4
7	0.377	0.856	0.55(56)	0.56(56)	86.2±0.4	5.8
8	0.373	0.850	0.62(56)	0.65(56)	83.4±0.4	6.1
9	0.372	0.848	0.96(56)	0.99(56)	85.0±0.4	6.6
10	0.364	0.839	1.00(56)	1.04(56)	82.8±0.6	6.3
11	0.343	0.830	0.82(56)	0.86(56)	85.9±1.0	8.3
12	0.340	0.832	0.57(56)	0.65(56)	87.7±0.7	8.5
13	0.339	0.830	0.74(56)	0.86(56)	89.1±0.7	9.1
14	0.339	0.833	0.69(56)	0.83(56)	90.7±0.7	8.9
15	0.338	0.839	0.65(56)	0.77(56)	91.2±0.7	9.0
16	0.338	0.840	0.76(56)	1.11(57)	93.0±0.7	8.9
17	0.334	0.850	0.73(56)	1.41(57)	100.9±1.4	8.8
18	0.329	0.857	0.98(56)	1.55(57)	108.4±1.1	8.9
19	0.321	0.858	0.62(56)	1.37(57)	106.7±0.9	8.9
20	0.322	0.861	0.47(56)	1.42(57)	104.7±0.8	9.1
21	0.295	0.835	0.73(56)	1.57(57)	69.4±0.6	10.6
22	0.282	0.812	0.62(56)	1.61(57)	56.7±0.7	11.3
23	0.258	0.768	0.77(56)	1.72(57)	42.0±0.9	12.4
24	0.233	0.726	1.06(56)	2.27(57)	25.6±1.4	13.9
25	0.220	0.702	1.61(56)	3.63(57)	20.9±1.2	15.2

¹ Western Model, i.e., wabs(bb+compTT+gauss).

² Eastern Model, i.e., wabs(diskbb+compTT+gauss).

³ R_{in} is derived from the Eastern Model in unit of km.